Electronic Supplementary Material (ESI) for New Journal of Chemistry.

Electronic Supplementary Information

Phosphorescent Pt(II) Complexes Bearing Cyclometalated Diflurophenylpyridinate and Diphosphine Building Blocks

Hamid R. Shahsavari, Samira Chamyani, Reza Babadi Aghakhanpour, Vahideh Dolatyari, and Sareh Paziresh*

Department of Chemistry, Institute for Advanced Studies in Basic Sciences (IASBS), Zanjan 45137-66731, Iran. * E-mail: shahsavari@iasbs.ac.ir.

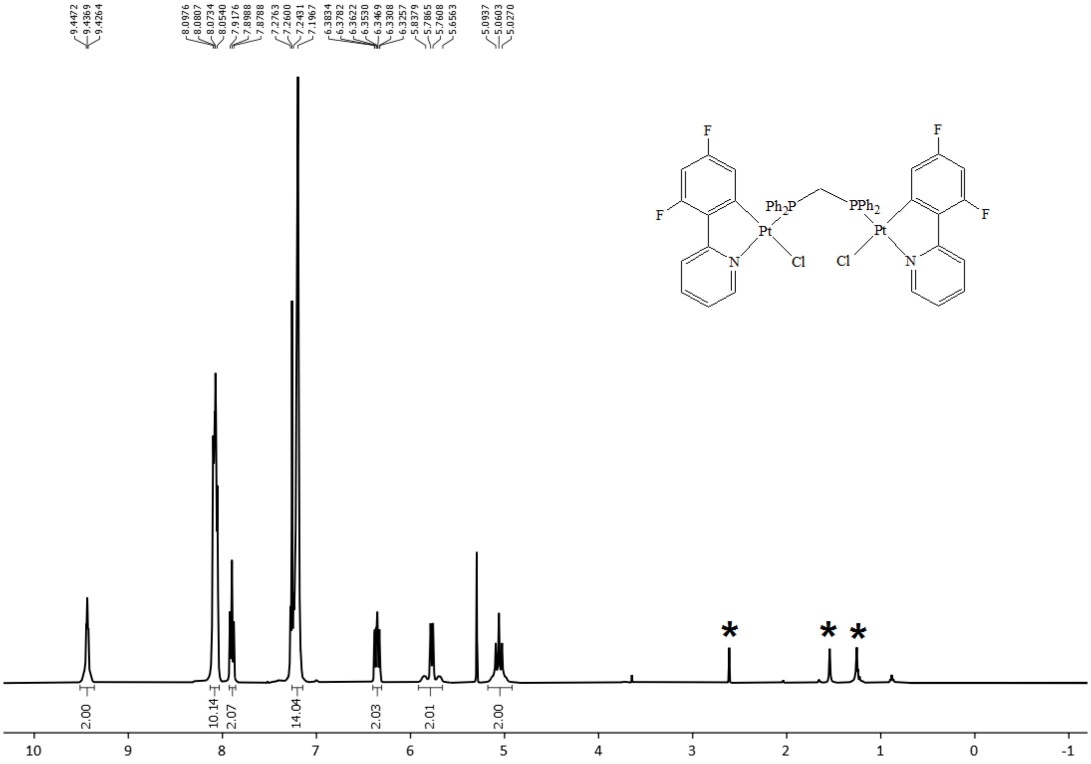

Figure S1. ^{1}H NMR spectrum of **3a** in CDCl$_3$ (* = residual solvent impurities).

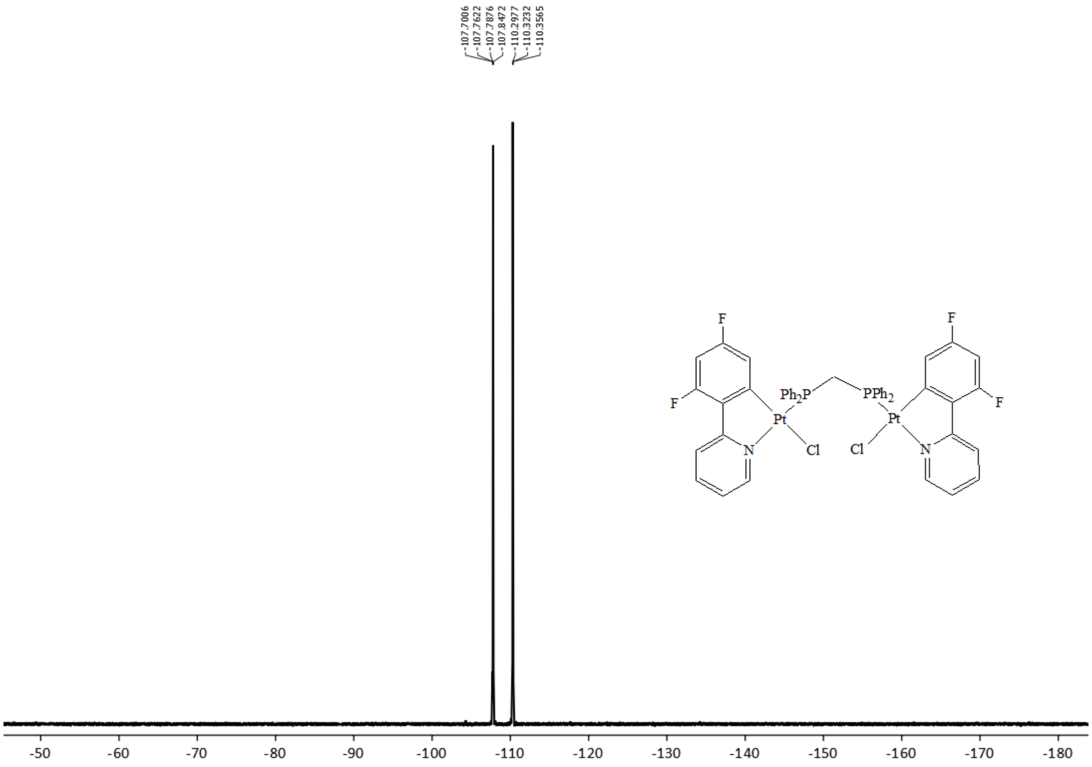

Figure S2. ^{19}F{^{1}H} NMR spectrum of **3a** in CDCl$_3$.

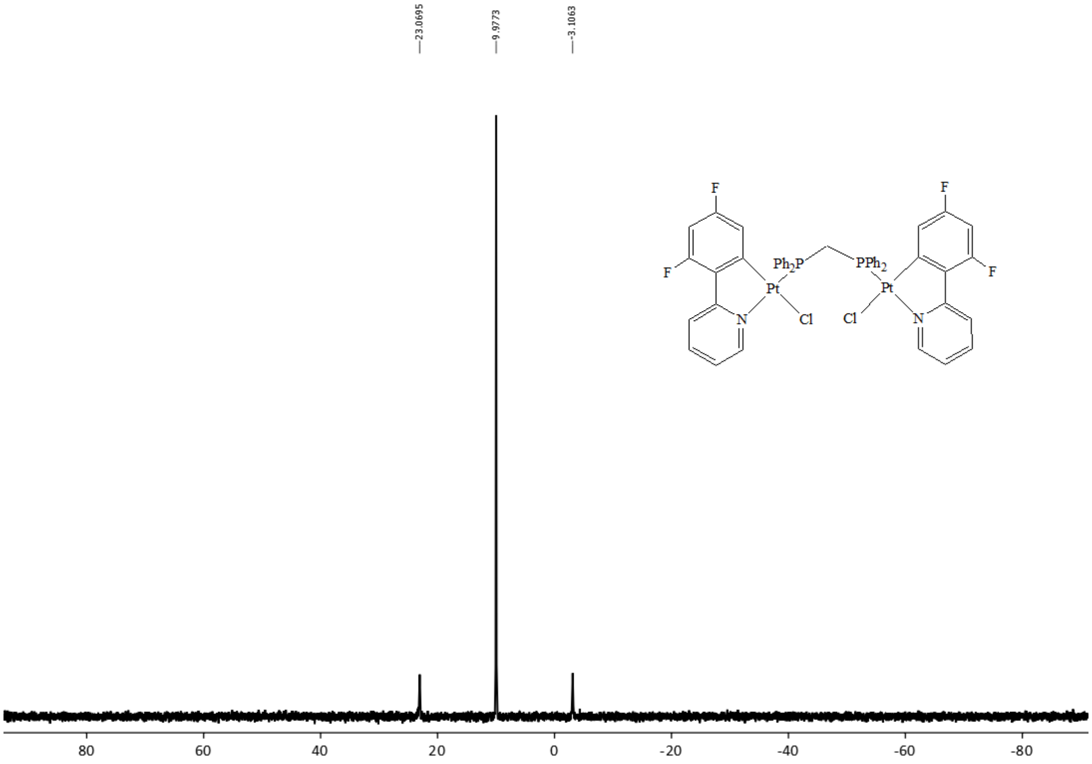

Figure S3. $^{31}P\{^1H\}$ NMR spectrum of **3a** in $CDCl_3$.

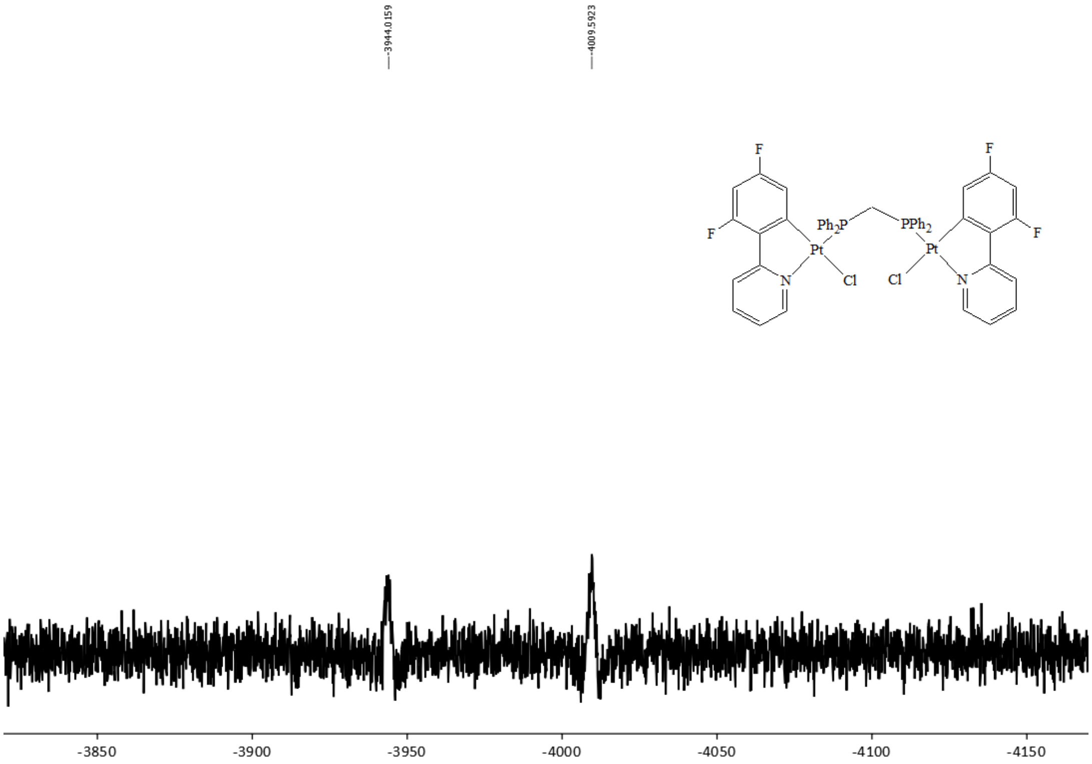

Figure S4. $^{195}Pt\{^1H\}$ NMR spectrum of **3a** in $CDCl_3$.

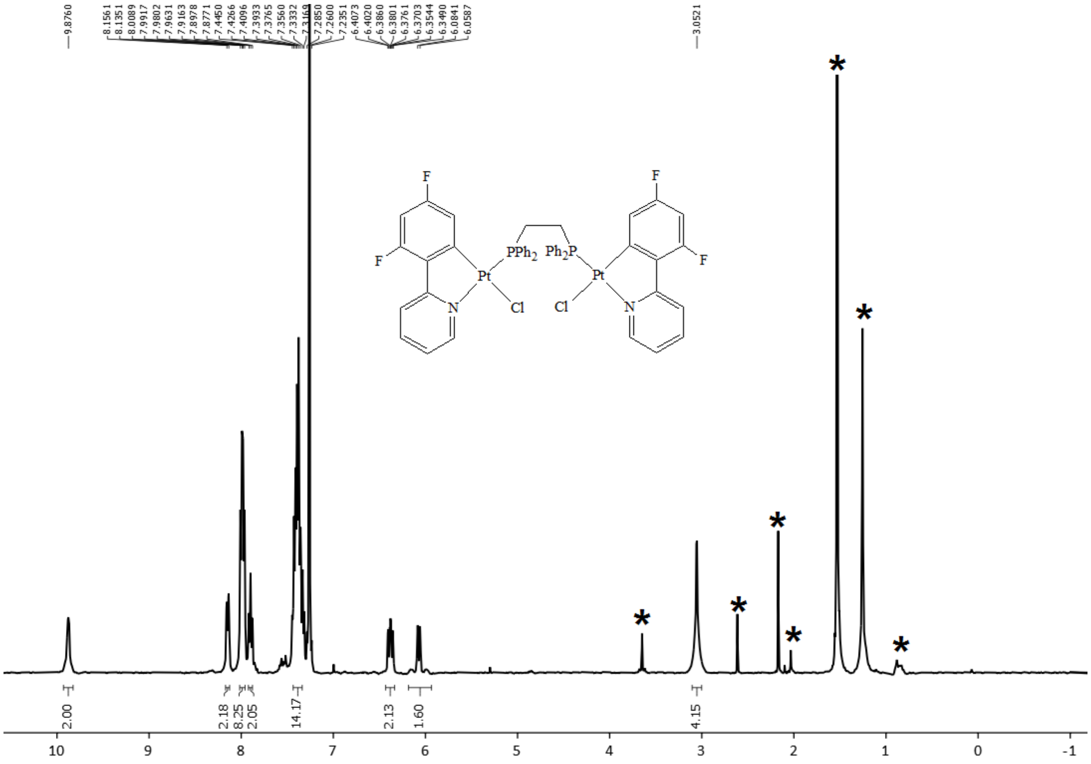

Figure S5. ^{1}H NMR spectrum of **3b** in $CDCl_3$ (* = residual solvent impurities).

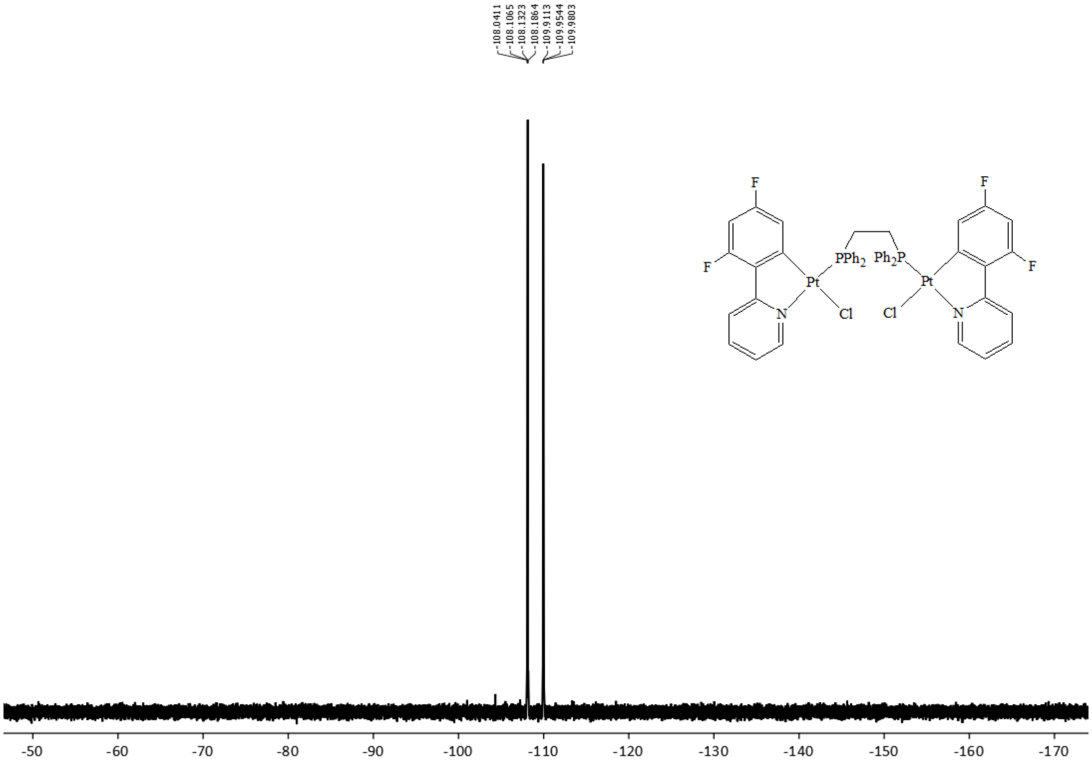

Figure S6. $^{19}F\{^1H\}$ NMR spectrum of **3b** in $CDCl_3$.

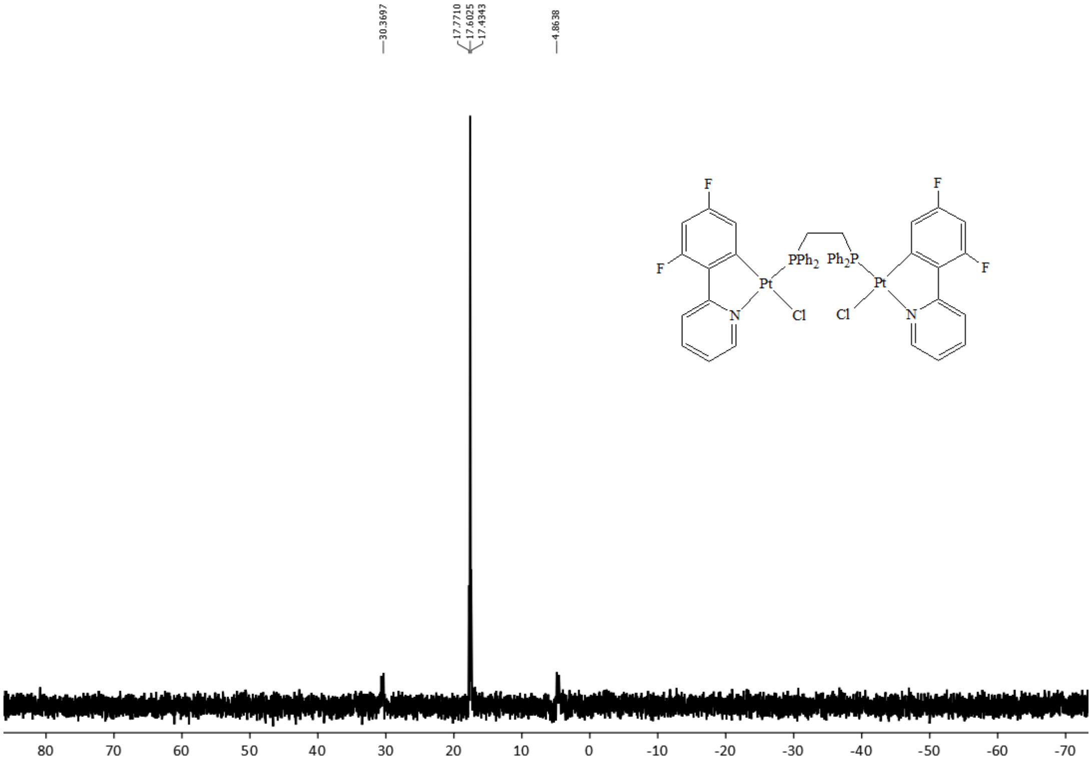

Figure S7. $^{31}P\{^1H\}$ NMR spectrum of **3b** in $CDCl_3$.

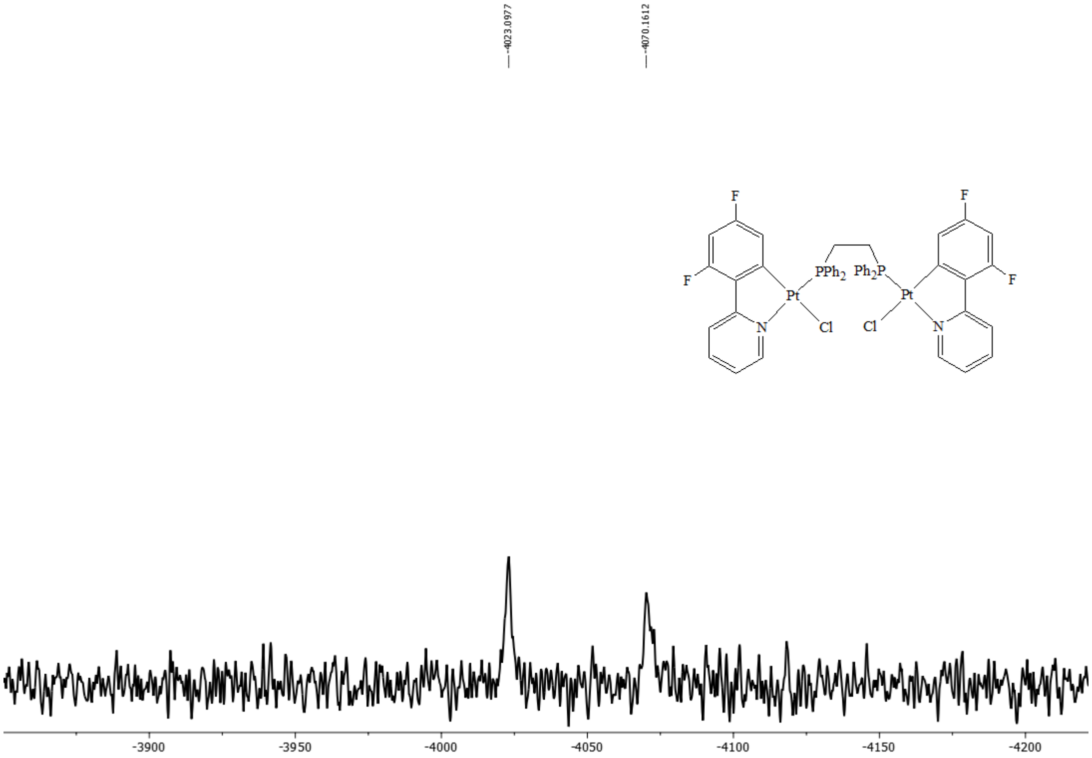

Figure S8. $^{195}Pt\{^1H\}$ NMR spectrum of **3b** in $CDCl_3$.

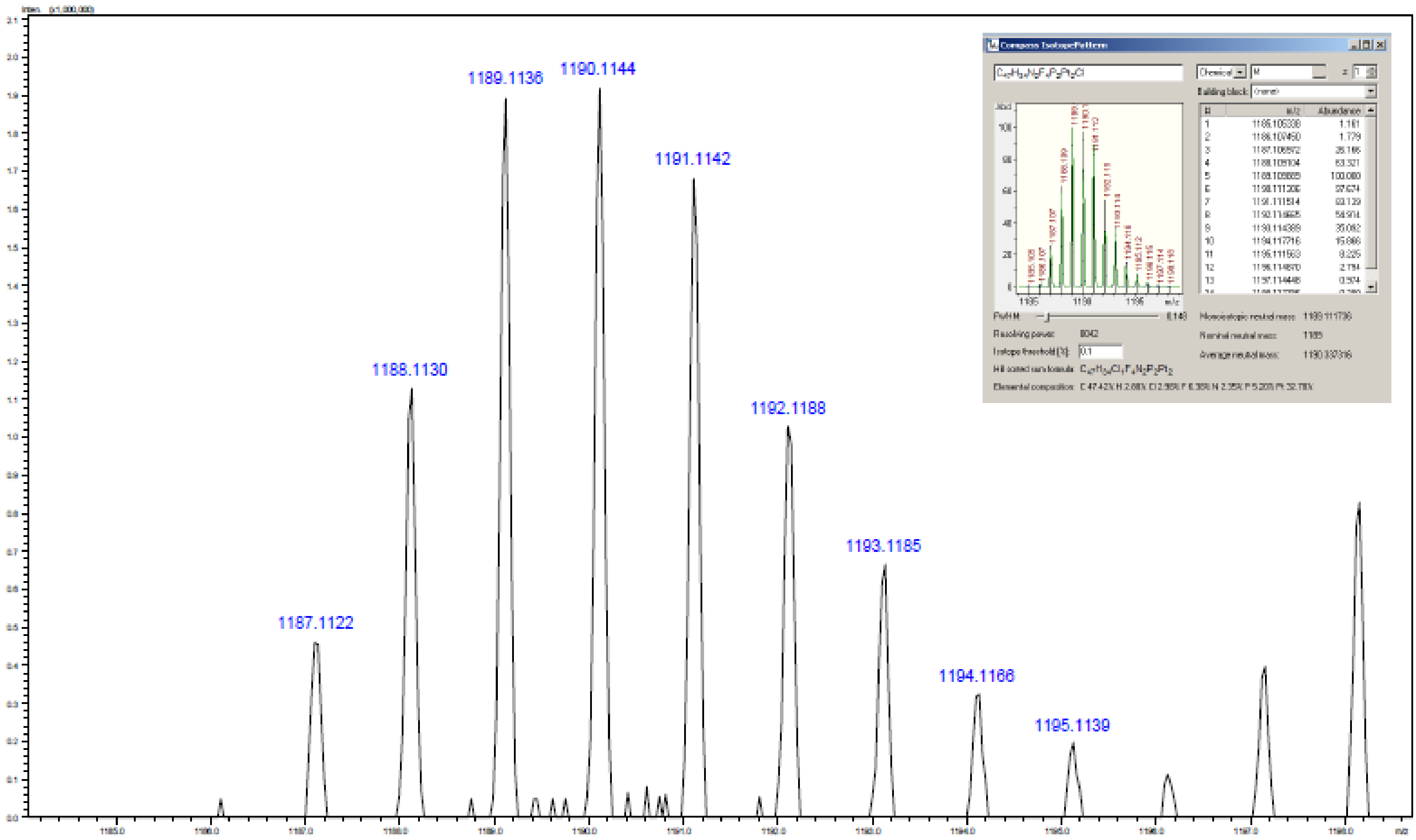

Figure S9. ESI-Mass spectrum of **3a** in CH_3CN.

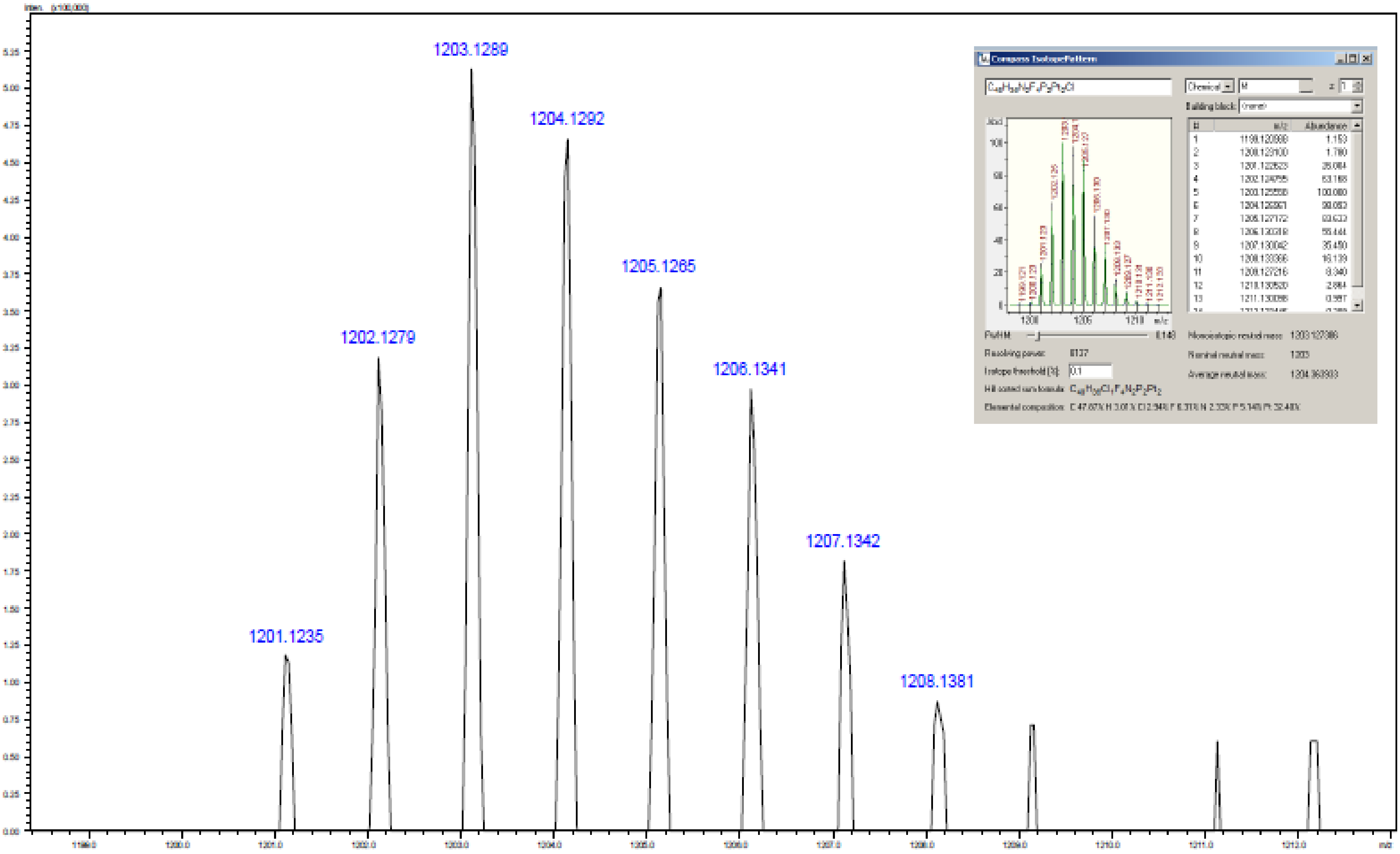

$C_{48}H_{36}N_2F_4P_2Pt_2Cl$

#	m/z	Abundance
1	1199.120898	1.153
2	1200.123100	1.780
3	1201.122623	28.084
4	1202.124795	63.168
5	1203.125558	100.000
6	1204.126261	98.082
7	1205.127172	93.633
8	1206.130218	55.441
9	1207.130042	35.450
10	1208.133066	16.139
11	1209.127216	8.340
12	1210.130520	2.884
13	1211.130098	0.987

Resolving power: 8137

Isotope threshold [%]: 0.1

Hill sorted sum formula: $C_{48}H_{36}Cl_1F_4N_2P_2Pt_2$

Elemental composition: C 47.87% H 3.01% Cl 2.94% F 6.31% N 2.33% P 5.14% Pt 32.40%

Monoisotopic neutral mass: 1203.127386

Nominal neutral mass: 1203

Average neutral mass: 1204.363933

Figure S10. ESI-Mass spectrum of **3b** in CH_3CN.

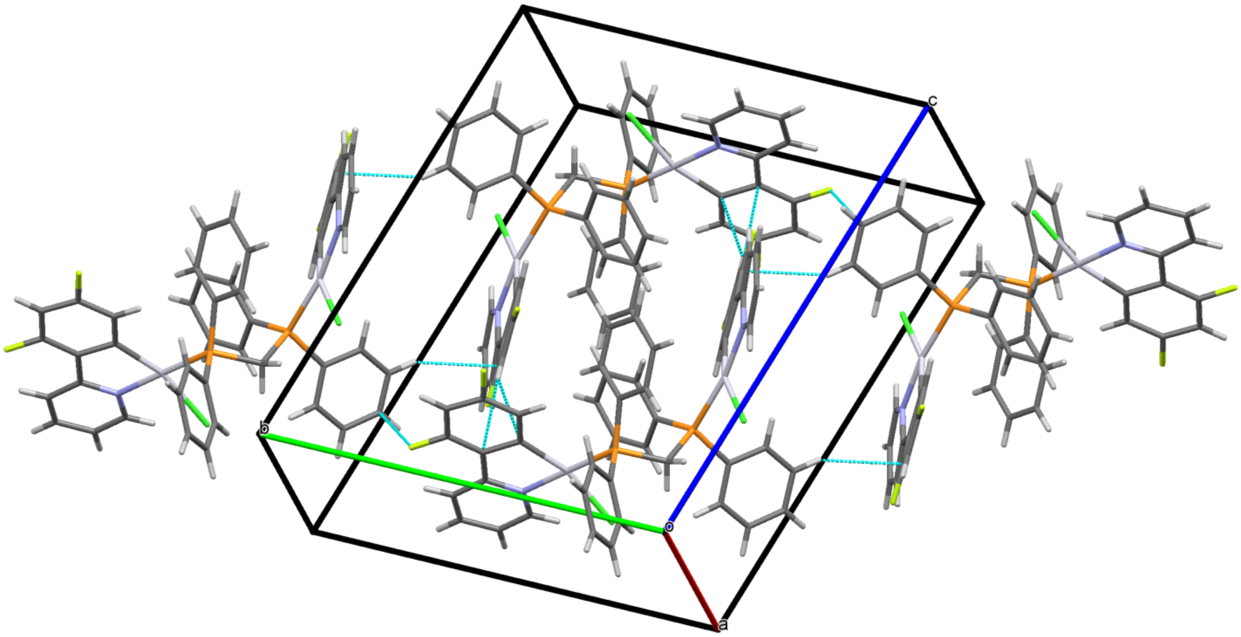

Figure S11. Crystal packing of the complex **3a**.

Table S1. Bond lengths [Å] and angles [°] for the crystal structure of **3a**.

Pt1-Cl1	2.3959(13)
Pt1-P1	2.2413(13)
Pt1-N1	2.081(4)
Pt1-C7	2.006(5)
Pt2-Cl2	2.3941(12)
Pt2-P2	2.2471(13)
Pt2-N2	2.077(4)
Pt2-C43	2.003(5)
P1-Pt1-Cl1	89.08(5)
N1-Pt1-Cl1	90.46(13)
N1-Pt1-P1	179.03(12)
C7-Pt1-Cl1	163.98(14)
C7-Pt1-P1	99.70(15)
C7-Pt1-N1	80.6(2)
P2-Pt2-Cl2	89.43(4)
N2-Pt2-Cl2	92.87(12)
N2-Pt2-P2	170.38(12)
C43-Pt2-Cl2	163.59(15)
C43-Pt2-P2	99.80(16)
C43-Pt2-N2	80.29(19)

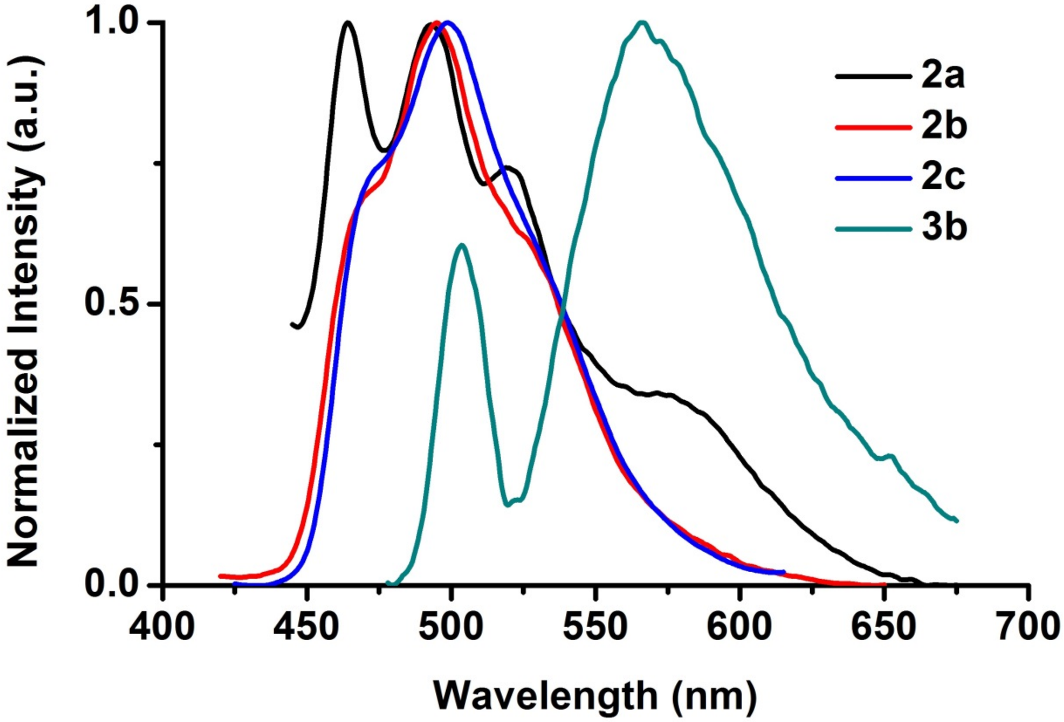

Figure S12. Emission spectra for **2a–c** and **3b** in PMMA at 298 K.

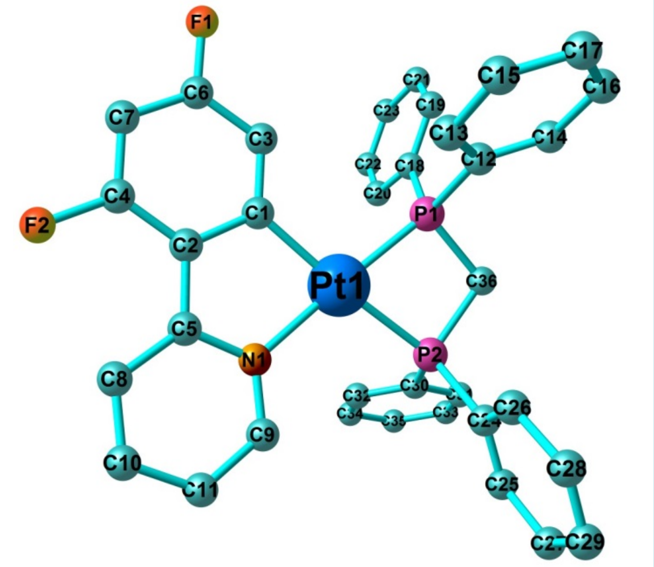

2a

Pt1-C1 (2.03945), Pt1-N1 (2.11166),
Pt1-P1 (2.31290), Pt1-P2 (2.43787),
C1-Pt1-N1 (80.11684), N1-Pt1-P2 (105.46061),
P2-Pt1-P1 (73.19318), P1-Pt1-C1 (101.56973).

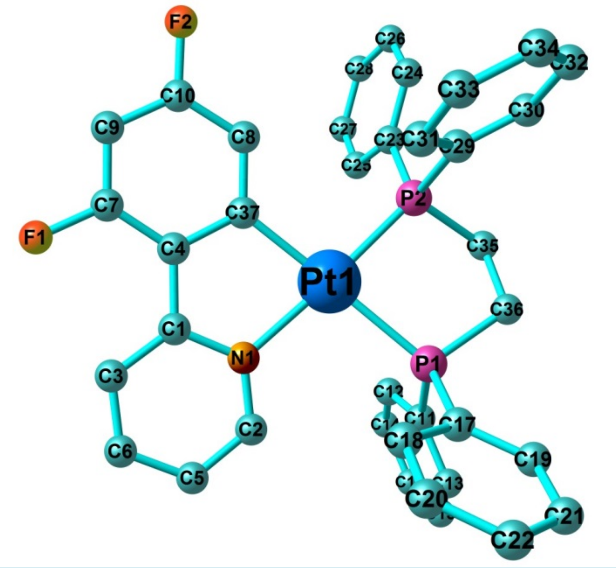

2b

Pt1-C37 (2.05634), Pt1-N1 (2.13103),
Pt1-P1 (2.43329), Pt1-P2 (2.31338),
C37-Pt1-N1 (79.68814), N1-Pt1-P1 (98.83510),
P1-Pt1-P2 (84.25518), P2-Pt1-C37 (97.63911).

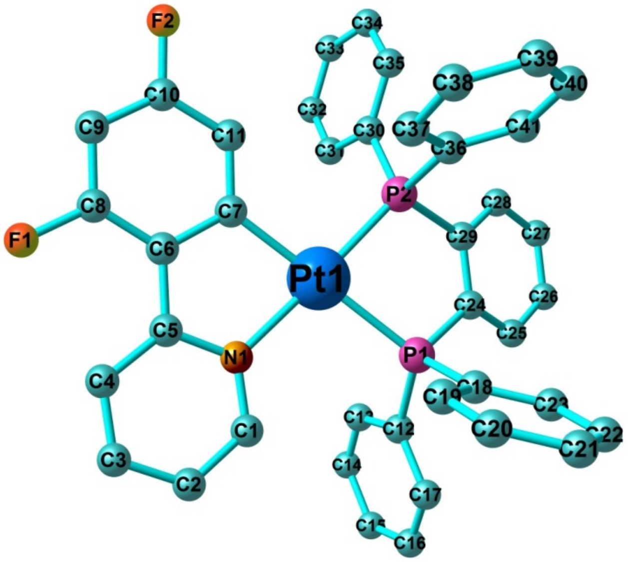

2c

Pt1-C7 (2.06122), Pt1-N1 (2.13166), Pt1-P1 (2.42909), Pt1-P2 (2.31673)
C7-Pt1-N1 (79.43564), N1-Pt1-P1 (99.69245), P1-Pt1-P2 (82.57105), P2-Pt1-C7 (98.29339)

Figure S13. View of the optimized structures of **2a-c** in gas phase (S_0) with atom numbering and selected bond distances (A°) and angles (deg).

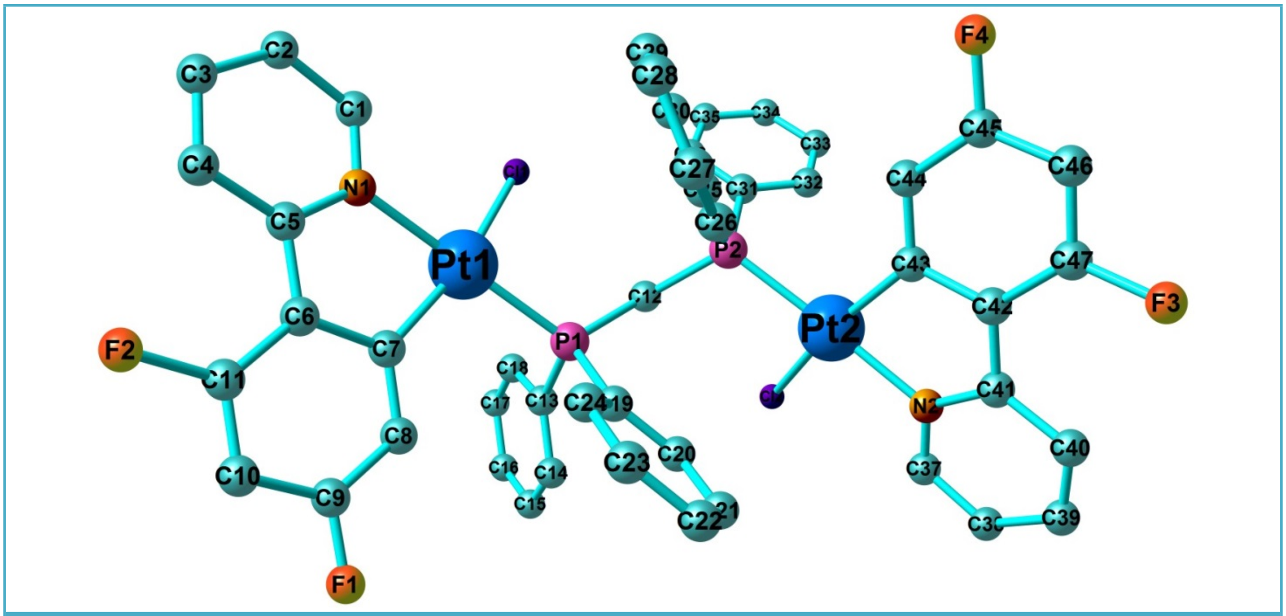

3a

Pt1-C7 (2.02165), Pt1-N1 (2.11806), Pt1-P1 (2.32933), Pt1-Cl1 (2.49192)
C7-Pt1-N1 (79.91095), N1-Pt1-Cl1 (91.80894), Cl1-Pt1-P1 (89.87728), P1-Pt1-C7 (89.87728)

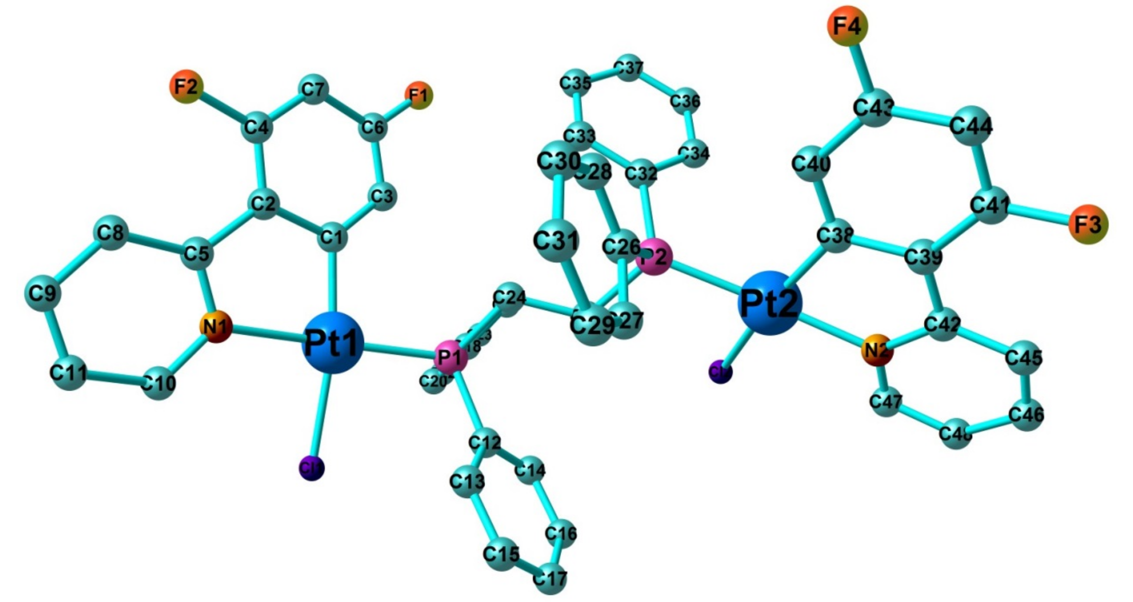

3b

Pt1-C1 (2.02075), Pt1-N1 (2.11625), Pt1-P1 (2.31333), Pt1-Cl1 (2.47454)
C1-Pt1-N1 (80.02011), N1-Pt1-Cl1 (92.00766), Cl1-Pt1-P1 (90.36339), P1-Pt1-C1 (98.00626)

Figure S14. View of the optimized structures of **3a-b** in gas phase (S_0) with atom numbering and selected bond distances (A°) and angles (deg).

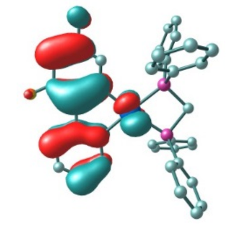	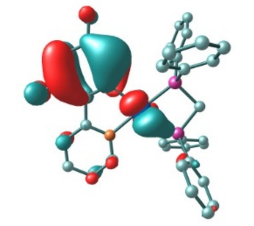	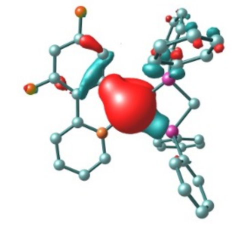
HOMO (-6.635 eV) Pt (19%), dfppy (79%) dppm (2%)	**HOMO-1 (-6.976 eV) Pt (22%), dfppy (71%) dppm (7%)**	**HOMO-2 (-7.036 eV) Pt (73%), dfppy (14%) dppm (13%)**
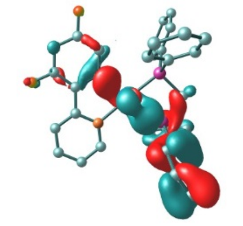	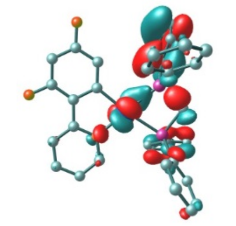	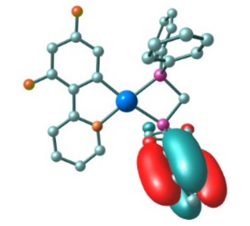
HOMO-3 (-7.241 eV) Pt (14%), dfppy (22%) dppm (64%)	**HOMO-4 (-7.438 eV) Pt (18%), dfppy (7%) dppm (75%)**	**HOMO-5 (-7.465 eV) Pt (0%), dfppy (1%) dppm (99%)**
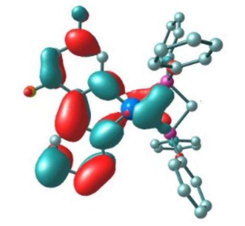	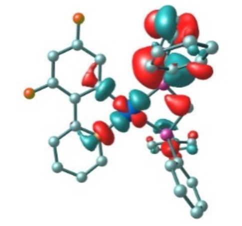	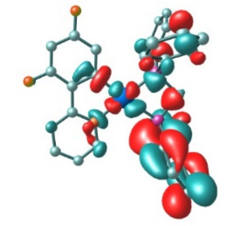
LUMO (-2.363 eV) Pt (7%), dfppy (73%) dppm (20%)	**LUMO+1 (-1.645 eV) Pt (20%), dfppy (12%) dppm (67%)**	**LUMO+2 (-1.561 eV) Pt (12%), dfppy (13%) dppm (75%)**
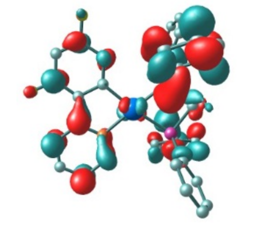	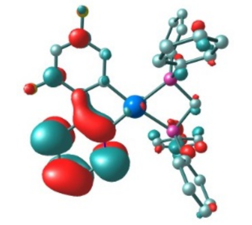	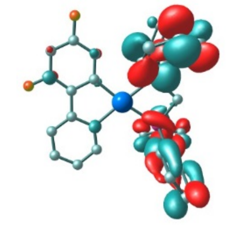
LUMO+3 (-1.540 eV) Pt (3%), dfppy (21%) dppm (76%)	**LUMO+4 (-1.410 eV) Pt (1%), dfppy (76%) dppm (23%)**	**LUMO+5 (-1.136 eV) Pt (13%), dfppy (6%) dppm (81%)**

Figure S15. Molecular orbital plots for the optimized structure of **2a** in CH_2Cl_2 solution with the energy levels and compositions.

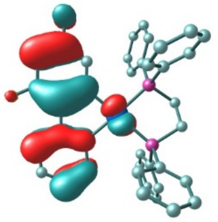	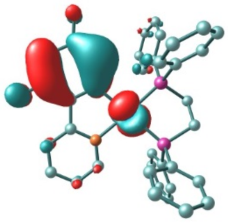	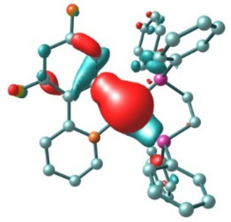
HOMO (-6.617 eV) **Pt (16%), dfppy (82%)** **dppe (2%)**	**HOMO-1 (-6.926 eV)** **Pt (28%), dfppy (64%)** **dppe (7%)**	**HOMO-2 (-7.021 eV)** **Pt (66%), dfppy (18%)** **dppe (14%)**
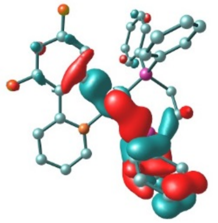	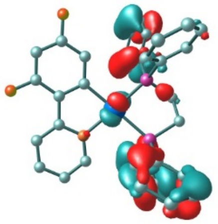	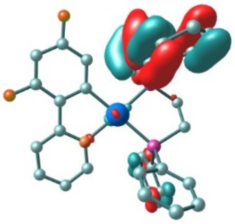
HOMO-3 (-7.277 eV) **Pt (15%), dfppy (20%)** **dppe (65%)**	**HOMO-4 (-7.450 eV)** **Pt (8%), dfppy (3%)** **dppe (89%)**	**HOMO-5 (-7.465 eV)** **Pt (3%), dfppy (2%)** **dppe (95%)**
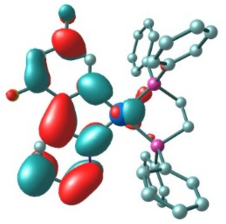	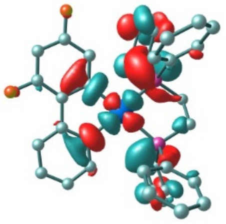	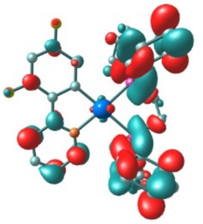
LUMO (-2.304 eV) **Pt (6%), dfppy (78%)** **dppe (15%)**	**LUMO+1 (-1.667 eV)** **Pt (22%), dfppy (17%)** **dppe (60%)**	**LUMO+2 (-1.501 eV)** **Pt (3%), dfppy (16%)** **dppe (81%)**
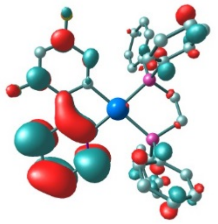	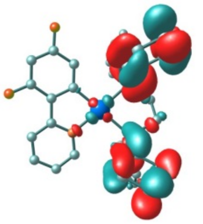	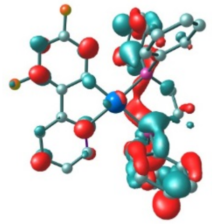
LUMO+3 (-1.400 eV) **Pt (1%), dfppy (74%)** **dppe (25%)**	**LUMO+4 (-1.275 eV)** **Pt (6%), dfppy (3%)** **dppe (91%)**	**LUMO+5 (-1.149 eV)** **Pt (8%), dfppy (14%)** **dppe (77%)**

Figure S16. Molecular orbital plots for the optimized structure of **2b** in CH_2Cl_2 solution with the energy levels and compositions.

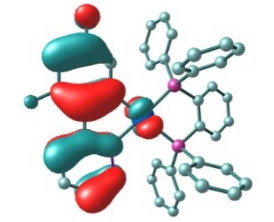	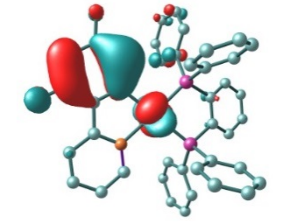	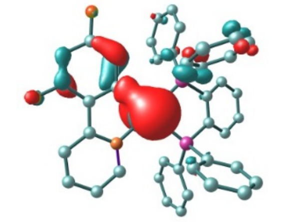
HOMO (-6.625 eV) **Pt (14%), dfppy (83%)** **dppb (3%)**	**HOMO-1 (-6.939 eV)** **Pt (29%), dfppy (54%)** **dppb (17%)**	**HOMO-2 (-7.008 eV)** **Pt (73%), dfppy (13%)** **dppb (15%)**
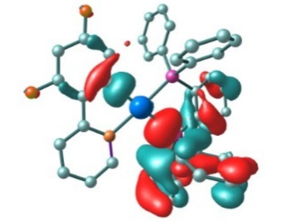	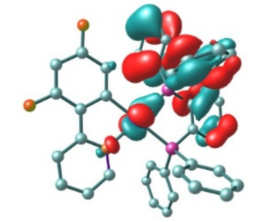	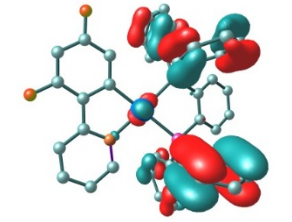
HOMO-3 (-7.160 eV) **Pt (6%), dfppy (24%)** **dppb (69%)**	**HOMO-4 (-7.411 eV)** **Pt (16%), dfppy (6%)** **dppb (78%)**	**HOMO-5 (-7.439 eV)** **Pt (5%), dfppy (3%)** **dppb (92%)**
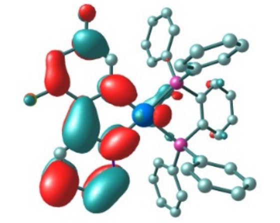	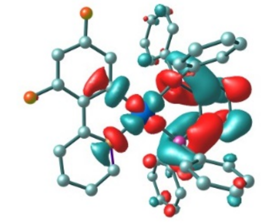	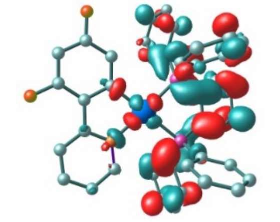
LUMO (-2.317 eV) **Pt (7%), dfppy (74%)** **dppb (19%)**	**LUMO+1 (-1.806 eV)** **Pt (19%), dfppy (12%)** **dppb (69%)**	**LUMO+2 (-1.687 eV)** **Pt (7%), dfppy (9%)** **dppb (84%)**
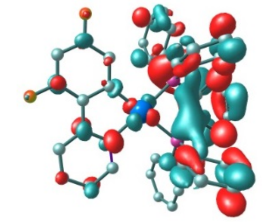	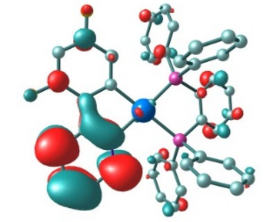	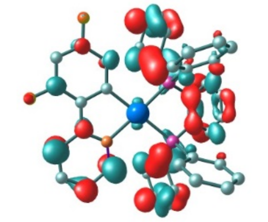
LUMO+3 (-1.640 eV) **Pt (6%), dfppy (11%)** **dppb (83%)**	**LUMO+4 (-1.412 eV)** **Pt (7%), dfppy (68%)** **dppb (26%)**	**LUMO+5 (-1.357 eV)** **Pt (9%), dfppy (17%)** **dppb (74%)**

Figure S17. Molecular orbital plots for the optimized structure of **2c** in CH_2Cl_2 solution with the energy levels and compositions.

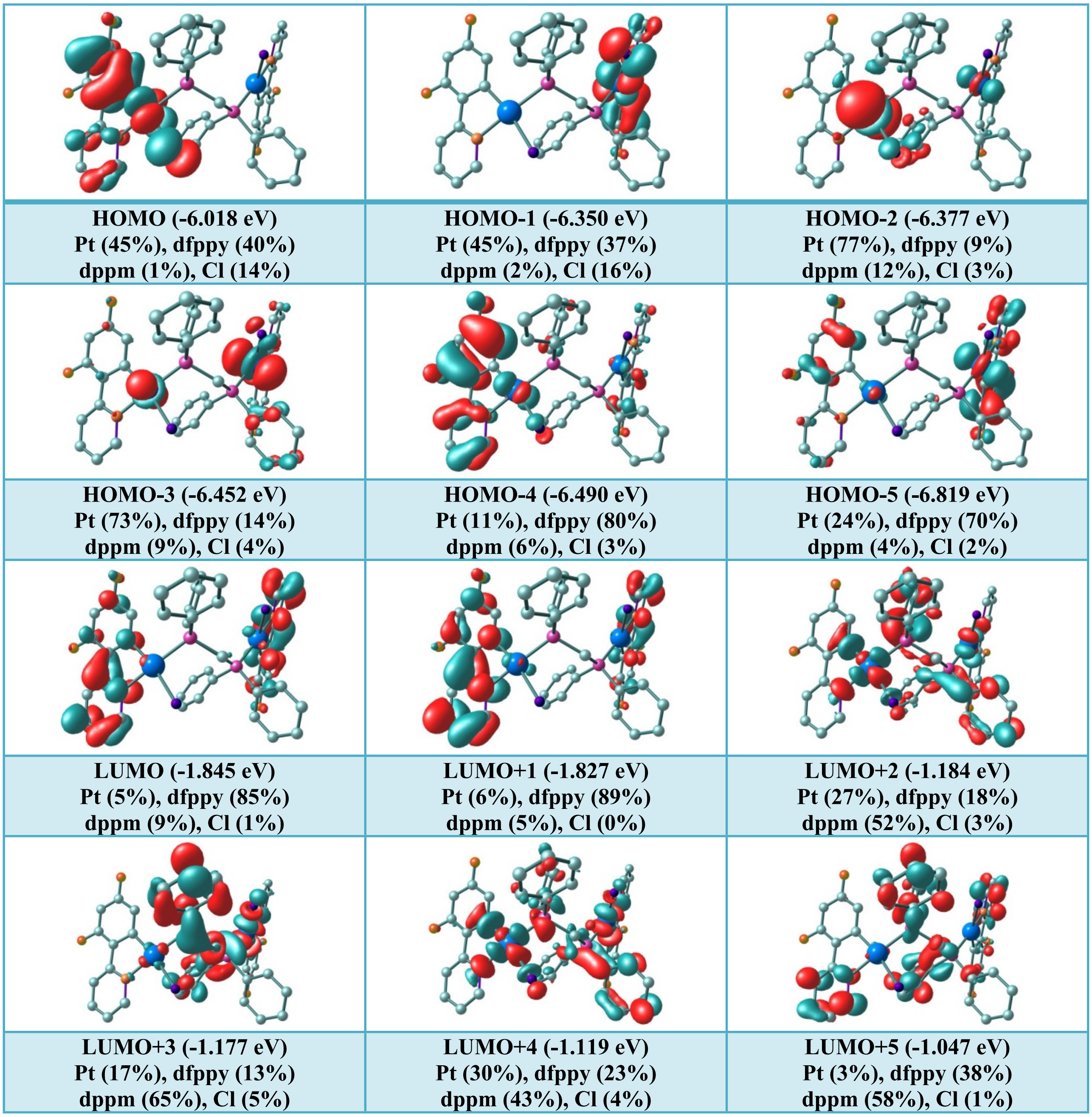

HOMO (-6.018 eV) **Pt (45%), dfppy (40%)** **dppm (1%), Cl (14%)**	**HOMO-1 (-6.350 eV)** **Pt (45%), dfppy (37%)** **dppm (2%), Cl (16%)**	**HOMO-2 (-6.377 eV)** **Pt (77%), dfppy (9%)** **dppm (12%), Cl (3%)**
HOMO-3 (-6.452 eV) **Pt (73%), dfppy (14%)** **dppm (9%), Cl (4%)**	**HOMO-4 (-6.490 eV)** **Pt (11%), dfppy (80%)** **dppm (6%), Cl (3%)**	**HOMO-5 (-6.819 eV)** **Pt (24%), dfppy (70%)** **dppm (4%), Cl (2%)**
LUMO (-1.845 eV) **Pt (5%), dfppy (85%)** **dppm (9%), Cl (1%)**	**LUMO+1 (-1.827 eV)** **Pt (6%), dfppy (89%)** **dppm (5%), Cl (0%)**	**LUMO+2 (-1.184 eV)** **Pt (27%), dfppy (18%)** **dppm (52%), Cl (3%)**
LUMO+3 (-1.177 eV) **Pt (17%), dfppy (13%)** **dppm (65%), Cl (5%)**	**LUMO+4 (-1.119 eV)** **Pt (30%), dfppy (23%)** **dppm (43%), Cl (4%)**	**LUMO+5 (-1.047 eV)** **Pt (3%), dfppy (38%)** **dppm (58%), Cl (1%)**

Figure S18. Molecular orbital plots for the optimized structure of **3a** in CH_2Cl_2 solution with the energy levels and compositions.

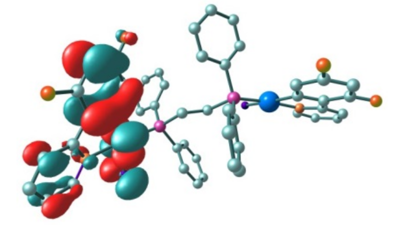	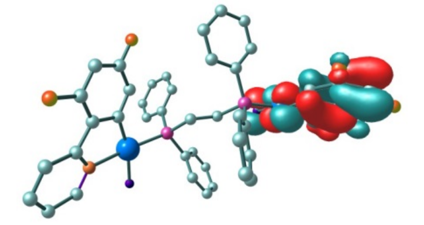	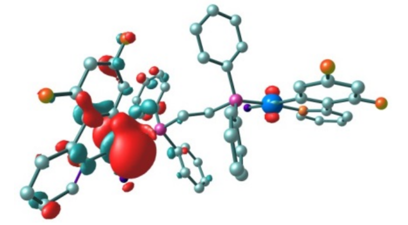
HOMO (-5.999 eV) **Pt (45%), dfppy (35%)** **dppe (1%), Cl (19%)**	**HOMO-1 (-6.020 eV)** **Pt (44%), dfppy (40%)** **dppe (0%), Cl (15%)**	**HOMO-2 (-6.390 eV)** **Pt (75%), dfppy (12%)** **dppe (11%), Cl (1%)**
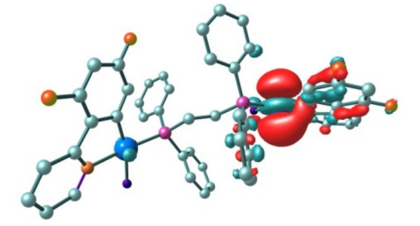	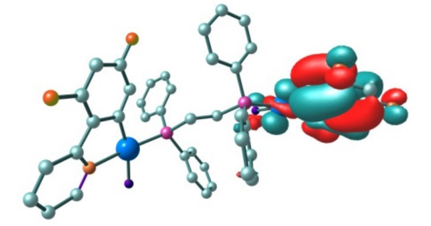	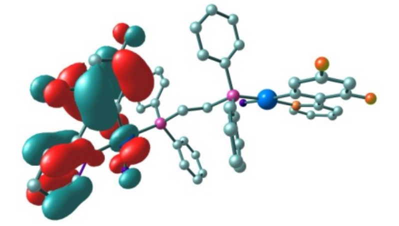
HOMO-3 (-6.458 eV) **Pt (80%), dfppy (11%)** **dppe (7%), Cl (2%)**	**HOMO-4 (-6.476 eV)** **Pt (18%), dfppy (74%)** **dppe (3%), Cl (4%)**	**HOMO-5 (-6.531 eV)** **Pt (21%), dfppy (72%)** **dppe (3%), Cl (5%)**
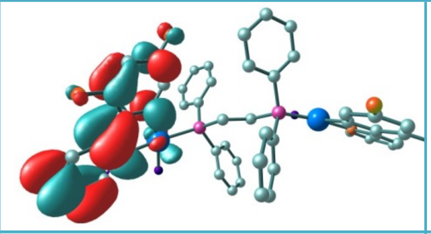	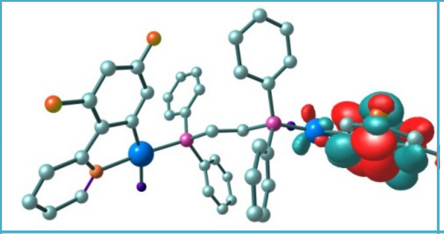	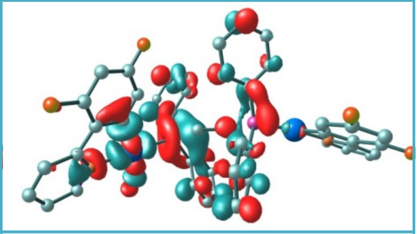
LUMO (-1.835 eV) **Pt (5%), dfppy (88%)** **dppe (6%), Cl (1%)**	**LUMO+1 (-1.826 eV)** **Pt (6%), dfppy (88%)** **dppe (5%), Cl (1%)**	**LUMO+2 (-1.273 eV)** **Pt (28%), dfppy (16%)** **dppe (53%), Cl (3%)**
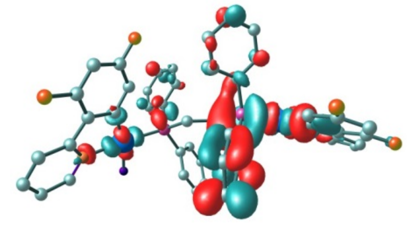	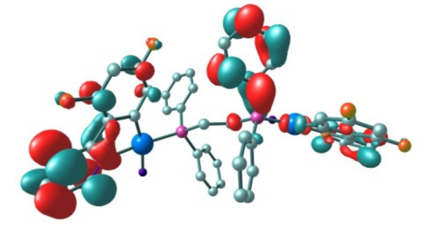	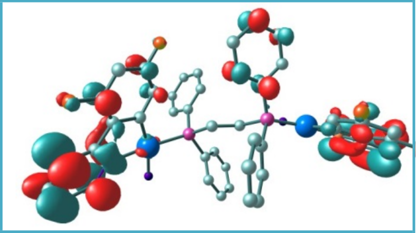
LUMO+3 (-1.194 eV) **Pt (30%), dfppy (18%)** **dppe (48%), Cl (3%)**	**LUMO+4 (-1.027 eV)** **Pt (4%), dfppy (57%)** **dppe (38%), Cl (1%)**	**LUMO+5 (-1.010 eV)** **Pt (3%), dfppy (80%)** **dppe (17%), Cl (0%)**

Figure S19. Molecular orbital plots for the optimized structure of **3b** in CH_2Cl_2 solution with the energy levels and compositions.

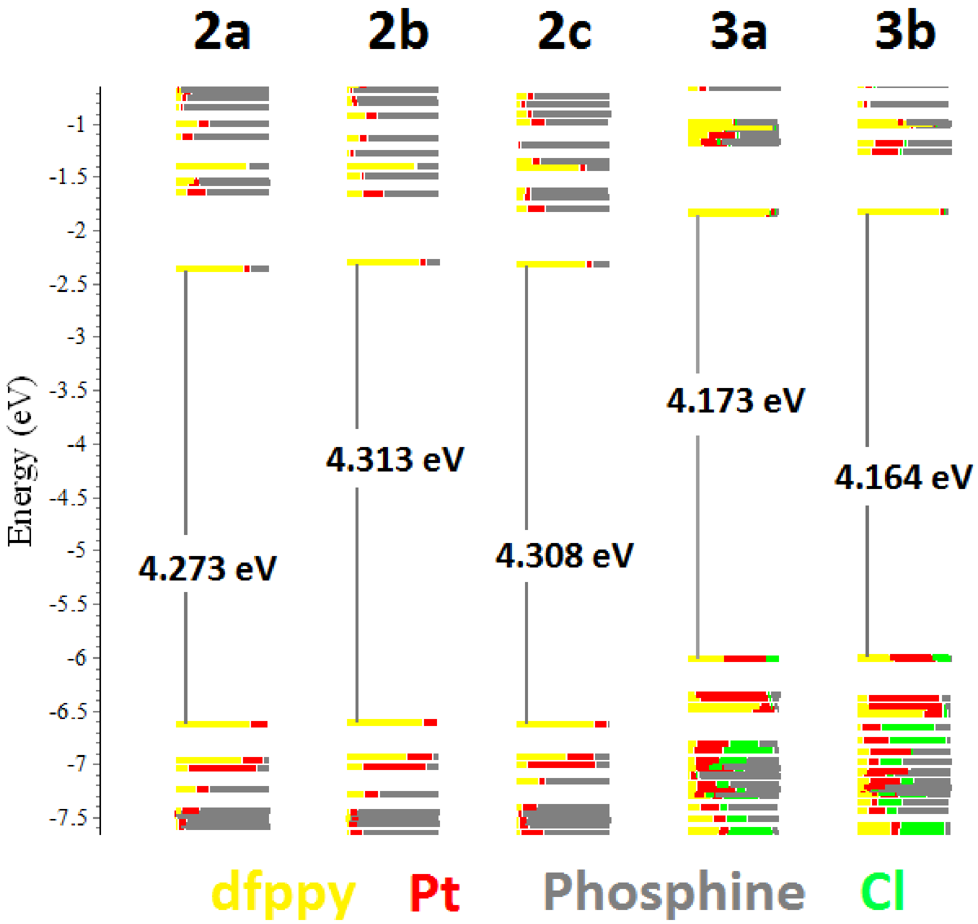

Figure S20. Comparative energy level diagram for the molecular orbitals of all the complexes.

Table S2. Wavelengths and the nature of transitions for **2a** where M = Pt, L = dfppy, L′ = dppm.

Excited state	λ(nm)	Osc. Strength	Major Contrib.	Assignment
1	349.5	0.0499	HOMO→LUMO (90%)	ILCT/ML′CT
3	313.4	0.1306	H-1→LUMO (85%)	ILCT/ML′CT
7	280.4	0.0583	H-10→LUMO (11%) H-4→LUMO (56%) HOMO→L+4 (10%)	L′LCT/MLCT L′LCT/MLCT ILCT/ML′CT
10	270.6	0.1312	H-1→L+1 (12%) HOMO→L+3 (60%)	LL′CT/ML′CT LL′CT/ML′CT
11	268.7	0.0021	H-5→LUMO (68%) HOMO→L+4 (13%)	IL′CT ILCT/ML′CT
13	266.6	0.0384	H-6→LUMO (78%) HOMO→L+4 (13%)	L′LCT/ IL′CT ILCT/ML′CT
15	263.5	0.0916	H-10→LUMO (10%) H-9→LUMO (29%) HOMO→L+4 (15%)	L′LCT/MLCT L′LCT/MLCT ILCT/ML′CT

Table S3. Wavelengths and the nature of transitions for **2b** where M = Pt, L = dfppy, L′ = dppe.

Excited state	λ(nm)	Osc. Strength	Major Contrib.	Assignment
1	343.9	0.0598	HOMO→LUMO (89%)	ILCT/ML′CT
3	311.8	0.1296	H-2→LUMO (11%) H-1→LUMO (76%)	MLCT ILCT/ML′CT
9	268.6	0.0907	HOMO→L+2 (78%)	LL′CT/ML′CT
12	264.8	0.0959	H-6→LUMO (20%) H-5→LUMO (40%) HOMO→L+3 (29%)	L′LCT L′LCT ILCT/ML′CT
13	263.3	0.0931	H-9→LUMO (12%) H-8→LUMO (14%) H-5→LUMO (31%) HOMO→L+3 (17%)	L′LCT L′LCT L′LCT ILCT/ML′CT

Table S4. Wavelengths and the nature of transitions for **2c** where M = Pt, L = dfppy, L′ = dppb.

Excited state	λ(nm)	Osc. Strength	Major Contrib.	Assignment
1	342.3	0.0701	HOMO→LUMO (89%)	ILCT/ML′CT
3	311.7	0.1229	H-2→LUMO (13%) H-1→LUMO (71%)	MLCT ILCT/ML′CT
9	276.8	0.0463	H-4→LUMO (14%) HOMO→L+3 (57%)	L′LCT LL′CT
10	276.0	0.0607	H-4→LUMO (22%) HOMO→L+2 (10%) HOMO→L+3 (26%) HOMO→L+4 (14%)	L′LCT LL′CT LL′CT ILCT/ML′CT
15	265.9	0.0901	H-6→LUMO (44%) H-3→L+1 (18%) HOMO→L+4 (16%)	L′LCT IL′CT ILCT/ML′CT
17	263.6	0.1084	H-7→LUMO (27%) HOMO→L+4 (33%)	L′LCT ILCT/ML′CT
25	256.5	0.0943	H-3→L+2 (42%) H-3→L+3 (16%)	IL′CT IL′CT
27	253.5	0.0971	H-3→L+2 (24%) H-3→L+3 (32%) H-2→L+4 (13%)	IL′CT IL′CT MLCT

Table S5. Wavelengths and the nature of transitions for **3a** where M = Pt, L = dfppy, L′ = dppm and X = Cl.

Excited state	λ (nm)	Osc. Strength	Major Contrib.	Assignment
1	363.6	0.0752	H-1→LUMO (57%) H-1→L+1 (26%)	ILCT/MLCT/XLCT ILCT/MLCT/XLCT
2	363.0	0.0288	HOMO→LUMO (36%) HOMO→L+1 (49%)	ILCT/MLCT/XLCT ILCT/MLCT/XLCT
11	307.9	0.121	H-4→LUMO (31%) H-4→L+1 (38%)	ILCT/MLCT ILCT/MLCT
12	307.3	0.1374	H-5→LUMO (42%) H-5→L+1 (18%)	ILCT/MLCT ILCT/MLCT
20	287.0	0.0752	H-1→L+5 (11%) H-1→L+6 (18%)	ILCT/ML′CT ILCT/MLCT
27	280.9	0.1247	H-8→LUMO (10%)	L′LCT/MLCT
28	278.6	0.0911	H-11→LUMO (10%) H-11→L+1 (13%)	L′LCT/MLCT L′LCT/MLCT

Table S6. Wavelengths and the nature of transitions for **3b** where M = Pt, L = dfppy, L′ = dppe and X = Cl.

Excited state	λ (nm)	Osc. Strength	Major Contrib.	Assignment
1	364.2	0.0547	HOMO→LUMO (94%)	ILCT/MLCT/XLCT
2	361.0	0.0571	H-1→L+1 (95%)	ILCT/MLCT/XLCT
11	305.8	0.0993	H-4→L+1 (68%)	ILCT/MLCT
12	305.2	0.116	H-6→LUMO (21%) H-5→LUMO (57%)	MLCT/XLCT L′LCT/MLCT
21	283.8	0.1904	H-8→LUMO (42%) HOMO→L+4 (10%) HOMO→L+5 (10%)	L′LCT/XLCT ILCT/ML′CT ILCT/ML′CT
28	275.0	0.2132	H-12→L+1 (12%) H-10→L+1 (37%)	L′LCT/MLCT/XLCT L′LCT/MLCT/XLCT

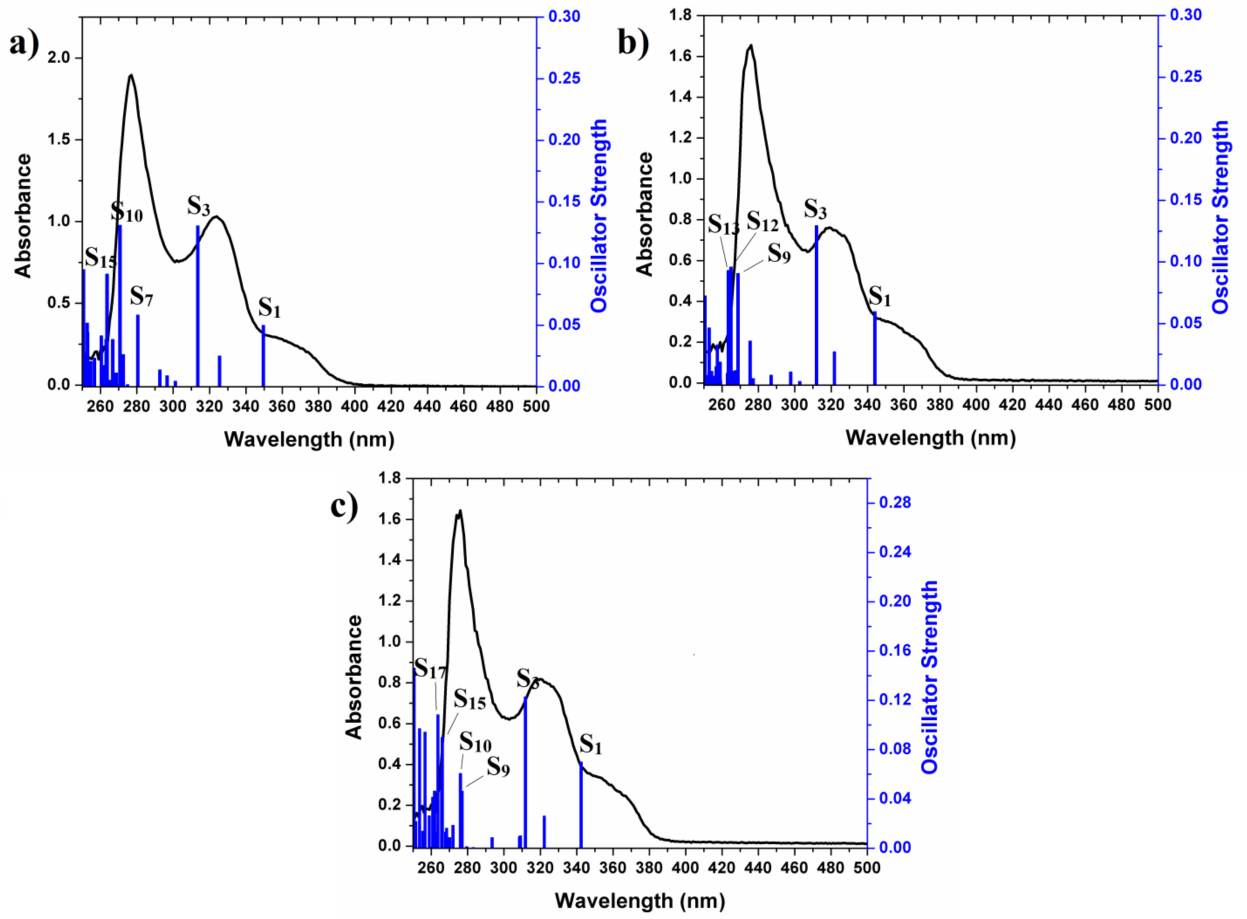

Figure S21. Overlaid experimental UV-Vis spectra and theoretical TD-DFT bars for a) **2a**, b) **2b** and c) **2c**.

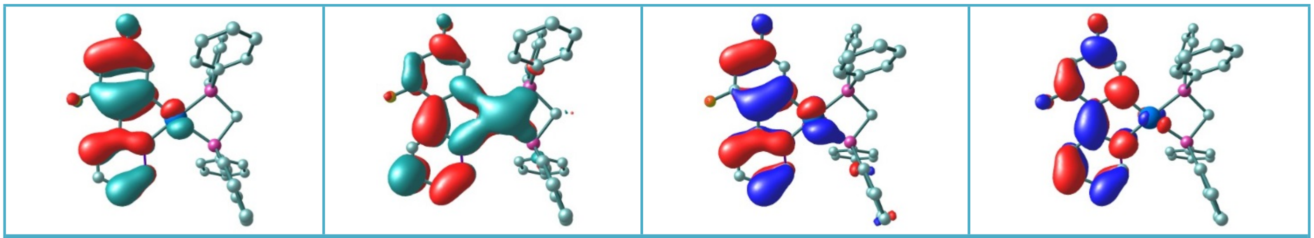

2a HOMO (-8.588 eV)

2a LUMO (-4.442 eV)

2a LSOMO (-8.933 eV)

2a HSOMO (-6.042 eV)

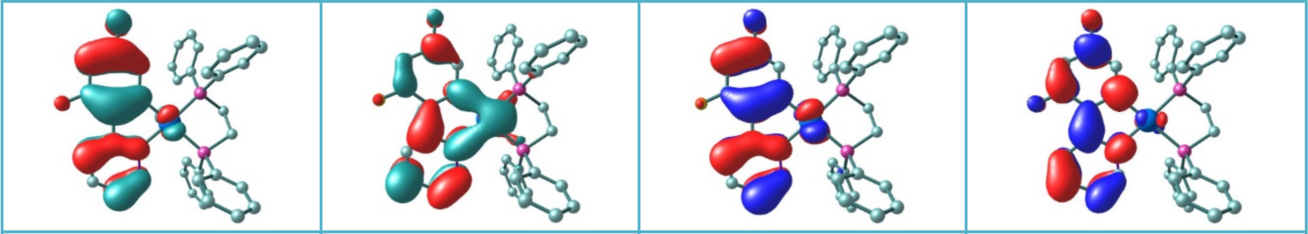

2b HOMO (-8.555 eV)

2b LUMO (-4.371 eV)

2b LSOMO (-8.913 eV)

2b HSOMO (-5.994 eV)

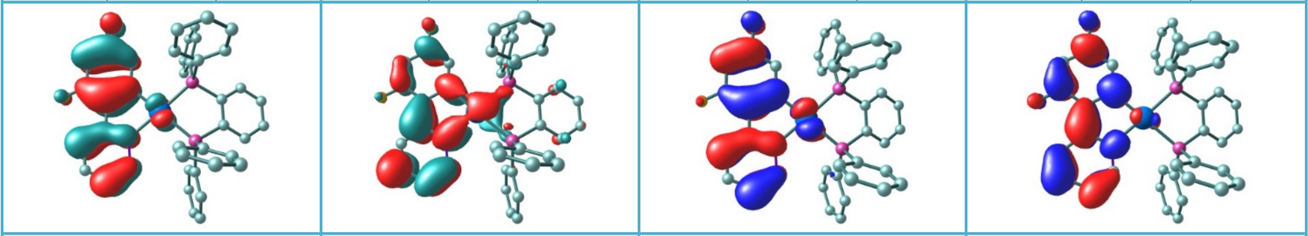

2c HOMO (-8.502 eV)

2c LUMO (-4.312 eV)

2c LSOMO (-8.849 eV)

2c HSOMO (-5.927 eV)

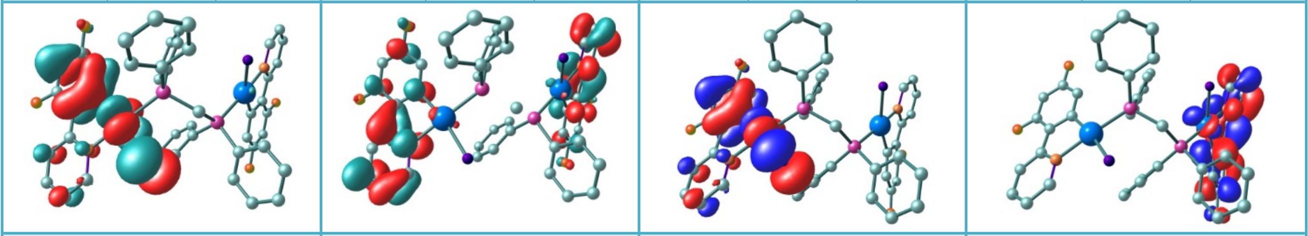

3a HOMO (-5.754 eV)

3a LUMO (-1.740 eV)

3a LSOMO (-5.773 eV)

3a HSOMO (-3.328 eV)

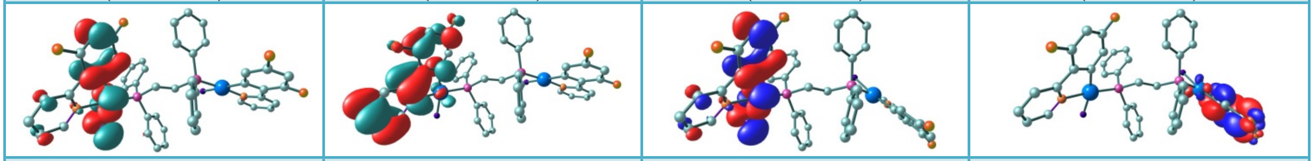

3b HOMO (-5.655 eV)

3b LUMO (-1.732 eV)

3b LSOMO (-5.671 eV)

3b HSOMO (-3.321 eV)

Figure S22. Frontier molecular orbital plots of **2a–c** and **3a-b** in S_0 and T_1 states (gas phase).

Table S7. Crystallographic and structure refinement data for **3a**.

3a	CCDC 2213060
Empirical formula	$C_{47}H_{34}Cl_2F_4N_2P_2Pt_2$
Formula weight	1225.78
Temperature/K	110.0
Crystal system	triclinic
Space group	P-1
a/Å	9.2890(3)
b/Å	13.9047(5)
c/Å	17.0859(6)
α/°	107.9010(10)
β/°	90.2110(10)
γ/°	105.9130(10)
Volume/Å^3	2010.17(12)
Z	2
ρ_{calc}g/cm^3	2.025
μ/mm^1	7.222
F(000)	1172.0
Crystal size/mm^3	0.4 × 0.2 × 0.1
Radiation	MoKα (λ = 0.71073)
2Θ range for data collection/°	2.516 to 57.416
Index ranges	$-12 \leq h \leq 12, -18 \leq k \leq 18, -23 \leq l \leq 23$
Reflections collected	84820
Independent reflections	10362 [$R_{int} = 0.0885, R_{sigma} = 0.0540$]
Data/restraints/parameters	10362/0/532
Goodness-of-fit on F^2	0.908
Final R indexes [I>=2σ (I)]	$R_1 = 0.0334, wR_2 = 0.0730$
Final R indexes [all data]	$R_1 = 0.0534, wR_2 = 0.0835$
Largest diff. peak/hole / e Å^{-3}	1.48/-1.85

Experimental Section

General procedures and materials

^{1}H NMR (400 MHz), ^{19}F{^{1}H} (376 MHz), ^{31}P{^{1}H} NMR (162 MHz) and ^{195}Pt{^{1}H} (86 MHz) spectra were recorded on a Bruker Avance 400 MHz instrument at 295 K. All chemical shifts (δ) are reported in ppm relative to their corresponding external standards ($SiMe_4$ for ^{1}H, $CFCl_3$ for ^{19}F{^{1}H}, 85% H_3PO_4 for ^{31}P{^{1}H}, Na_2PtCl_6 for ^{195}Pt{^{1}H}) and the coupling constants (*J*) have being expressed in Hz. The instrument for HR ESI-Mass measurement was a Shimadzu IT-TOF with an electrospray ionization source, which is part of the Arkansas Statewide Mass Spectrometry Facility. UV-Vis spectra were performed using a Perkin-Elmer Lambda 25 spectrophotometer. Photoluminescence spectra were recorded on a Perkin-Elmer LS45 fluorescence spectrometer at room and low temperatures. The luminescence lifetime values were determined in the phosphorimeter mode. Luminescence quantum yield values (Φ) were evaluated using an integrated sphere method. The 2-(2,4-difluorophenyl)pyridine (dfppy), bis(diphenylphosphino)methane (dppm), 1,2-bis(diphenylphosphino)ethane (dppe) and 1,2-bis(diphenylphosphino)benzene (dppbz) and all the other chemicals were purchased from commercial resources. All the reactions were carried out under Argon atmosphere and in the common solvents and all the solvents were purified and dried according to standard procedures.[1]

X-ray Crystallography

Single crystals of **3a** were obtained by slow diffusion of *n*-hexane into its CH_2Cl_2 solution at room temperature. A suitable crystal was selected for structural analysis and intensity data for **3a** were collected using a Bruker APEX-II CCD diffractometer. The crystal was kept at 110.0 K during data collection. Using Olex2,[2] the structure was solved with the ShelXT[3] structure solution program using Intrinsic Phasing and refined with the ShelXL[4] refinement package using Least Squares minimization. The crystallographic data and refinement parameters are summarized in Table S7.

Computational Details

Density functional calculations were performed with the program suite Gaussian 09[5] using the B3LYP level of theory.[6-8] The LANL2DZ basis set was chosen to describe Pt[9, 10] and the 6-31G(d) basis set was chosen for other atoms. The geometries of complexes were fully optimized by employing the density functional theory without imposing any symmetry constraints. In order to ensure the optimized geometries, frequency calculations were performed employing analytical second derivatives. Time-dependent DFT (TD-DFT) calculations were carried out at the same level of theory and basis sets. Solvent effects have been considered by the conductor-like polarizable continuum model (CPCM)[11, 12]. The calculations for the electronic absorption spectra by time-dependent DFT (TD-DFT) were performed at the same level of theory.

References

1. Armarego, W. L. F., Purification of Laboratory Chemicals. 8th ed.; Butterworth-Heinemann 2017.

2. Dolomanov, O. V.; Bourhis, L. J.; Gildea, R. J.; Howard, J. A. K.; Puschmann, H., OLEX2: A Complete Structure Solution, Refinement and Analysis Program. *J. Appl. Cryst.* **2009**, *42*, 339-341.

3. Sheldrick, G., SHELXT-Integrated Space-group and Crystal-structure Determination. *Acta Cryst.* **2015**, *A71*, 3-8.

4. Sheldrick, G., Crystal Structure Refinement with SHELXL. *Acta Cryst.* **2015**, *C71*, 3-8.

5. Frisch, M. J.; Trucks, G. W.; Schlegel, H. B.; Scuseria, G. E.; Robb, M. A.; Cheeseman, J. R.; Scalmani, G.; Barone, V.; Mennucci, B.; Petersson, G. A.; Nakatsuji, H.; Caricato, M.; Li, X.; Hratchian, H. P.; Izmaylov, A. F.; Bloino, J.; Zheng, G.; Sonnenberg, J. L.; Hada, M.; Ehara, M.; Toyota, K.; Fukuda, R.; Hasegawa, J.; Ishida, M.; Nakajima, T.; Honda, Y.; Kitao, O.; Nakai, H.; Vreven, T.; Montgomery, J. J. A.; Peralta, J. E.; Ogliaro, F.; Bearpark, M.; Heyd, J. J.; Brothers, E.; Kudin, K. N.; Staroverov, V. N.; Keith, T.; Kobayashi, R.; Normand, J.; Raghavachari, K.; Rendell, A.; Burant, J. C.; Iyengar, S. S.; Tomasi, J.; Cossi, M.; Rega, N.; Millam, J. M.; Klene, M.; Knox, J. E.; Cross, J. B.; Bakken, V.; Adamo, C.; Jaramillo, J.; Gomperts, R.; Stratmann, R. E.; Yazyev, O.; Austin, A. J.; Cammi, R.; Pomelli, C.; Ochterski, J. W.; Martin, R. L.; Morokuma, K.; Zakrzewski, V. G.; Voth, G. A.; Salvador, P.; Dannenberg, J. J.; Dapprich, S.; Daniels, A. D.; Farkas, O.; Foresman, J. B.; Ortiz, J. V.; Cioslowski, J.; Fox, D. J., *Gaussian 09, Revision A.02*. 2016; p Gaussian, Inc., Wallingford CT.

6. Becke, A. D., Density-functional Thermochemistry. III. The Role of Exact Exchange. *J. Chem. Phys.* **1993**, *98*, 5648-5652.

7. Miehlich, B.; Savin, A.; Stoll, H.; Preuss, H., Results Obtained with the Correlation Energy Density Functionals of Becke and Lee, Yang and Parr. *Chem. Phys. Lett.* **1989**, *157*, 200-206.

8. Lee, C.; Yang, W.; Parr, R. G., Development of the Colle-Salvetti Correlation-Energy Formula into a Functional of the Electron Density. *Phys. Rev. B* **1988**, *37*, 785.

9. Wadt, W. R.; Hay, P. J., Ab Initio Effective Core Potentials for Molecular Calculations. Potentials for Main Group Elements Na to Bi. *J. Chem. Phys.* **1985**, *82*, 284-298.

10. Roy, L. E.; Hay, P. J.; Martin, R. L., Revised Basis Sets for the LANL Effective Core Potentials. *J. Chem. Theory Comput.* **2008**, *4*, 1029-1031.

11. Cossi, M.; Scalmani, G.; Rega, N.; Barone, V., New Developments in the Polarizable Continuum Model for Quantum Mechanical and Classical Calculations on Molecules in Solution. *J. Chem. Phys.* **2002**, *117*, 43-54.

12. Barone, V.; Cossi, M.; Tomasi, J., A New Definition of Cavities for the Computation of Solvation Free Energies by the Polarizable Continuum Model. *J. Chem. Phys.* **1997**, *107*, 3210-3221.